THE JOURNAL OF PHYSICAL CHEMISTRY C

pubs.acs.org/JPCC

Article

Revisiting a Perovskite-like Copper-Formate Framework $NH_4[Cu(HCOO)_3]$: Order−Disorder Transition Influenced by Jahn-Teller Distortion and above Room-Temperature Switching of the Nonlinear Optical Response between Two SHG-Active States

Paulina Peksa, Jan K. Zaręba,* Maciej Ptak, Mirosław Mączka, Anna Gągor, Sebastian Pawlus, and Adam Sieradzki*

Cite This: *J. Phys. Chem. C* 2020, 124, 18714−18723

Read Online

ACCESS | Metrics & More | Article Recommendations | Supporting Information

ABSTRACT: Metal-formate frameworks comprising ammonium cations as guests are proven to be a fertile ground to study various phenomena associated with the temperature-induced changes in structural, dielectric, optical, and magnetic properties. In this contribution, we revisit $NH_4[Cu(HCOO)_3]$, a member of metal formates that distinguishes itself in terms of its phase transition behavior and associated properties. New data on structural dynamics of all phases of $NH_4[Cu(HCOO)_3]$ have been obtained with the use of variable-temperature Raman measurements. Smooth changes of band positions observed near 220 K attest to the postulated continuous nature of low-temperature phase transition, whereas apparent discontinuities at 355 K confirm the first-order type of transition between orthorhombic (II) and hexagonal (I) phases. Low-temperature Raman data were confronted with diffraction results, pointing to a significant effect of Jahn-Teller distortion on the vibrational properties the CuO_6 subnetwork. In the high-temperature range, a significant broadening of bands is observed, confirming that phase I is highly disordered, with the strongest changes of full width at half maximum (FWHM) parameters being observed for bands corresponding to NH_4^+ cations. Dielectric investigations revealed the symmetric shape of the observed process indicating the Debye-like relaxation. Thus, the dielectric relaxation was characterized in terms of the dipolar relaxation model using the Cole−Cole relaxation function, leading to an E_a value of approximately 0.76 eV. Finally, temperature-resolved second harmonic generation (SHG) measurements unequivocally corroborate the noncentrosymmetric setting of phases II and I, as well as allowed us to realize temperature-induced switching of second-order nonlinear optical (NLO) responses. We demonstrate that $NH_4[Cu(HCOO)_3]$ serves as a host to uncommon kind of quadratic NLO switching, which takes advantage of two SHG-active states: SHG-*high* state below T_c, and SHG-*low* state above T_c. The demonstrated SHG-*high* − SHG-*low* temperature-driven bistability stands out from the vast majority of molecular and coordination polymer NLO switches that employ binary SHG-*on* and SHG-*off* switching schemes.

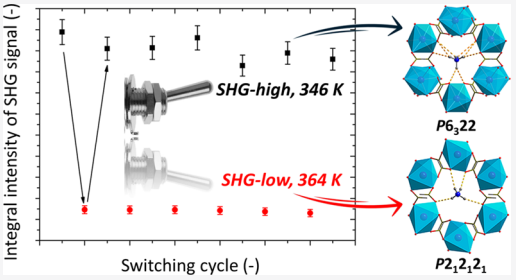

INTRODUCTION

Metal−organic frameworks (MOFs) are under constant scrutiny of scientific community owing to the broad scope of technologically relevant applications.[1−6] One of the emerging subclasses of MOFs is protonated amine-templated metal-formate frameworks. Metal-formate frameworks can be described with a general formula of $cat[M^{II}(HCOO)_3]$ in which *cat* stands for monoprotonated ammonium (NH_4^+), dimethylammonium ($(CH_3)_2NH_2^+$), guanidinium ($(H_2N)_3C^+$), etc., while M^{II} stands for a divalent metal ion (e.g., Mg, Zn, Mn, Ni, Co, Fe, and Cu). These materials enjoyed widespread attention by virtue of their unique properties that are appealing from the fundamental science point of view but also may constitute the basis for the preparation of functional materials, drawing from their multiferroic properties and phase transition behavior, particularly of order−disorder nature.[7−14]

Accumulated structural data on metal formates reveal that the combinations of ammonium cations as protonated bases with M^{II} cations afford 3D coordination chiral frameworks whose topological type can be described by the $4^9 \cdot 6^6$ point symbol, crystallizing in the hexagonal $P6_322$ space group (phase I).[15−17] From the coordination chemistry point of view, these compounds are built from metal centers of octahedral disposition, which are connected by formate ligands in an *anti−anti* coordination geometry. The phase transition properties are largely imparted by the temperature-dependent dynamic

Received: July 5, 2020
Revised: July 28, 2020
Published: August 2, 2020

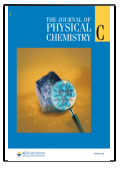

behavior of NH_4^+ guest molecules that occupy channels of the host metal-formate framework. Their interaction with the coordination network rests on the hydrogen-bonding (HB) interactions with oxygen acceptors of formate units (N−H···O). The metal ion itself was found to have a profound effect on the phase transition properties as well. Depending on the metal ion employed, the T_c of high-temperature phase transition falls into the range of 192−355 K. The presence of noncentrosymmetric, polar order in turn offers the possibility for ferroelectric ordering, and indeed, distinct ferroelectric properties have been demonstrated for the $NH_4[Zn(HCOO)_3]$ formate framework.[18] On the other hand, the change of the metal center may afford disparate electrical properties; for example, antiferroelectricity has been demonstrated for the title compound, $\mathbf{NH_4[Cu(HCOO)_3]}$.[19] Likewise, magnetic ordering is also strongly dependent on the metal ion involved, e.g., ferromagnetic exchange between metal centers was determined for $NH_4[Co(HCOO)_3]$ and $NH_4[Ni(HCOO)_3]$, whereas the antiferromagnetic order was identified for $\mathbf{NH_4[Cu(HCOO)_3]}$ and $NH_4[Mn(HCOO)_3]$.[16] As can be seen, $\mathbf{NH_4[Cu(HCOO)_3]}$ combines antiferroelectric and antiferromagnetic properties, positioning this material as a multiferroic member of the metal-formate family. From the structural viewpoint, it is known that the transition from the hexagonal antiferroelectric phase to high-temperature, helical one (space group $P2_12_12_1$ of the orthorhombic system, phase II) takes place at $T_c = 355$ K and has the first-order character; note that this is the highest T_c among all ammonium-based metal formates. At low temperatures, in turn, temperature-induced structural changes have continuous character and are related to rather subtle modifications of the coordination environment of Cu^{2+}, essentially being a structural manifestation of the Jahn-Teller effect. Although properties of these phase transitions and associated crystal phases have been probed using several experimental methods, there are still some gaps in the knowledge on peculiar features of the phase behavior of $\mathbf{NH_4[Cu(HCOO)_3]}$. First, no closer details on the mechanism of low-temperature phase transition have been provided, possibly due to the fact that signatures of anomalous behavior in structural and dielectric measurements were weakly marked in previously published data. Second, in an earlier study, no clear anomaly in DSC traces was observed at the low-temperature region, suggesting that the energetic effect due to phase transition could be within the experimental accuracy of the performed calorimetric measurement. Third, the dispersion in frequency-dependent dielectric measurements, although observed, was not associated with any specific dielectric relaxation process. Fourth, up to now, there was no insight into temperature-resolved vibrational characteristics of $\mathbf{NH_4[Cu(HCOO)_3]}$.

This paper aims to fill all the above gaps in knowledge on the phase properties of $\mathbf{NH_4[Cu(HCOO)_3]}$. To this end, a detailed reinvestigation of thermal properties (DSC) and structural (X-ray single crystal diffraction) and dielectric spectroscopy in temperature and frequency domains is performed. These studies are complemented by temperature-dependent Raman measurements that provide another perspective on structural dynamics of $\mathbf{NH_4[Cu(HCOO)_3]}$. Moreover, the noncentrosymmetric character of both orthorhombic and hexagonal phases, although well documented using X-ray diffraction methods, has not been verified so far using any independent experimental technique. Accordingly, we have performed temperature-resolved second harmonic generation (TR-SHG) measurements on $\mathbf{NH_4[Cu(HCOO)_3]}$, which not only corroborated the noncentrosymmetric character of these phases but also allowed us to identify this material as potentially useful for temperature-induced nonlinear optical (NLO) switching. Specifically, we found that the SHG response of $\mathbf{NH_4[Cu(HCOO)_3]}$ can be switched between two SHG-active states: the SHG-*high* state below T_c and SHG-*low* state above T_c, thus being much different from vast majority NLO switches that employ discrete SHG-*on* and SHG-*off* logic states.

EXPERIMENTAL SECTION

Synthesis. In order to obtain $\mathbf{NH_4[Cu(HCOO)_3]}$ crystals, the slow diffusion technique was applied and is an adaptation of a previously reported synthetic protocol of related metal-formate compounds.[15,16] In this procedure, 12 mmol (0.7567 g) of $HCOONH_4$ and ca. 26.5 mmol (1 mL) of HCOOH (98% aq. sol.) were dissolved in 15 mL of CH_3OH and transferred to a glass tube (9 mm inner diameter). The second solution (less dense) composed of 1.5 mmol (0.2017 g) of $CuCl_2$ in 15 mL of CH_3OH was gently dropped into the tube to obtain a liquid−liquid interface between the two solutions. The glass tube was sealed and left undisturbed. The blue crystals of $\mathbf{NH_4[Cu(HCOO)_3]}$, grown on the surface of the tube, were harvested after 1 week, washed three times with methanol, and dried at 50 °C in air.

X-ray Single-Crystal Diffraction. The single-crystal X-ray diffraction was performed on an Xcalibur Atlas diffractometer operating with Mo K_α radiation. The data were collected at temperatures ranging from 295 to 120 K. CrysAlisPro and CrysAlisRed (Rigaku Oxford Diffraction, 2015) were used for data collection and processing. The crystal structures were solved and refined using SHELXT 2014/5 and SHELXL 2018/3. The details concerning the crystal, data collection, and refinement at 230 and 120 K are given in Table S1 in the Supplementary Information, together with the selected bonds and angles (Table S2 in the Supporting Information) and HB geometry (Table S3 in the Supporting Information). Thermal evolution of lattice parameters is presented in Figure S1 in the Supporting Information.

Differential Scanning Calorimetry (DSC). The heat-flow thermograms were measured using a high-resolution 0.04 μW Mettler Toledo DSC-1 calorimeter. Nitrogen was used as a purging gas. The measurements were performed in the 130−390 K temperature range, and the heating and cooling rate was 5 K/min. The excess heat capacity associated with the phase transition was evaluated by subtraction from the data the baseline representing variation in the absence of the phase transitions.

Raman Spectroscopy. The temperature-dependent Raman spectra were measured in the 80−380 K range in a Linkam THMS600 cryostat cell using a Renishaw InVia Raman spectroscope equipped with a confocal DM 2500 Leica optical microscope, a thermoelectrically cooled CCD as a detector, and an argon laser operating at 488 nm.

Dielectric Properties. The dielectric measurements at ambient pressure were performed using a Novocontrol Alpha impedance analyser. Samples were surrounded by the silver paste, which was used to ensure a good electrical contact. The AC voltage with amplitude to 1 V and frequency in the range 10^6−10^{-1} Hz were applied across the sample. The temperature was controlled with a Novocontrol Quattro system, by using a nitrogen gas cryostat. All dielectric measurements were

https://dx.doi.org/10.1021/acs.jpcc.0c06141
J. Phys. Chem. C 2020, 124, 18714−18723

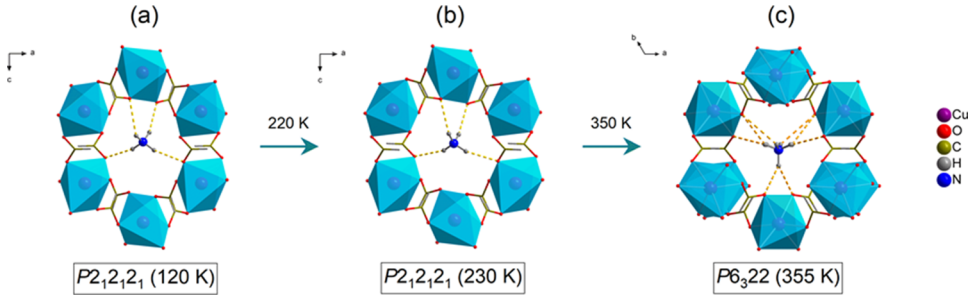

Figure 1. Projections of structural motifs present in $NH_4[Cu(HCOO)_3]$ projected along in successive phases at (a) 120 K (along the *b* axis), (b) 230 K (along the *b* axis), and (c) 355 K (along the *c* axis). Dashed lines denote N−H···O HBs, and blue polyhedra represent coordination spheres of Cu^{2+} ions. Projection for 355 K was drawn using a previously reported crystal structure.[16]

performed every 1 K over the temperature range from 130 to 390 K.

Second-Harmonic Generation (SHG). SHG studies were performed using a laser system consisting of a Quantronix Integra-C regenerative amplifier operating as an 800 nm pump and a Quantronix-Palitra-FS BIBO crystal-based optical parametric amplifier (OPA). This system delivers wavelength-tunable pulses of ∼130 fs length and operates at a repetition rate of 1 kHz. For temperature-resolved SHG (TR-SHG) studies and the Kurtz-Perry powder test, we have used the output from a Quantronix-Palitra-FS femtosecond OPA set to 1250 nm wavelength. The Kurtz-Perry powder test at 800 nm was performed using attenuated output from the Quantronix Integra-C regenerative amplifier. Prior to measurements, the single crystals of $NH_4[Cu(HCOO)_3]$ and potassium dihydrogen phosphate (KDP, used as a reference for the Kurtz-Perry test, were crushed with a spatula and sieved through a mini-sieve set (Aldrich), collecting a microcrystal size fraction of 88−125 μm. Next, size-graded samples of $NH_4[Cu(HCOO)_3]$ and KDP were fixed between microscope glass slides (forming tightly packed layers), sealed, and mounted to the holder. In all experiments, the laser beam was directed onto samples at 45° and was unfocused. Signal-collecting optics, mounted to the glass optical fiber, was placed perpendicularly to the plane of the sample (backscattering geometry). Scattered pumping radiation was suppressed with the use of a 700 nm short pass dielectric filter (FESH0700, Thorlabs). Attenuation of laser beam intensity was performed with the use of reflective mirror. Spectra of SHG signals were recorded with Ocean Optics Flame T and Ocean Optics QE Pro-FL spectrographs.

TR-SHG study (from 298 to 373 K for heating run and from 373 to 298 K for cooling run, with a 2−3 K step) was conducted using a 1250 nm unfocused beam of 99 mW mean power. Temperature control was performed using a thermostated heating plate (Heidolph). Temperature switching of SHG was performed by setting the temperature at 346 and 364 K in an alternate manner, and at these temperature points, the $NH_4[Cu(HCOO)_3]$ sample was irradiated using the same beam parameters used for TR-SHG study.

Assessment of the SHG efficiency of $NH_4[Cu(HCOO)_3]$ at 298 K was performed with the use of the Kurtz-Perry technique using KDP as a reference.[20,21] This test was performed at 1250 nm (average beam power of 105 mW) and 800 nm (average beam power of 240 mW). For the test at 1250 nm, the spectra were collected for 800 ms, for both KDP and $NH_4[Cu(HCOO)_3]$, whereas at 800 nm, the spectra were collected for 1000 and 5000 ms for KDP and $NH_4[Cu(HCOO)_3]$, respectively.

RESULTS AND DISCUSSION

Crystal Structure. Structural data for $NH_4[Cu(HCOO)_3]$ have been previously reported by Shang et al.[16] Briefly, $NH_4[Cu(HCOO)_3]$ comprises a chiral $[Cu(HCOO)_3]$ 3D framework of the $4^9{\cdot}6^6$ topological type. Channels are occupied by NH_4^+ amines, and Cu^{2+} ions feature distorted octahedral coordination with four short basal Cu−O bonds and two elongated apical ones. Metal centers are interconnected via formate nodes in *anti*−*anti* connection mode. The room temperature phase is orthorhombic with the $P2_12_12_1$ space group, whereas the high-temperature polymorph adopts hexagonal $P6_322$ symmetry. Figure 1 illustrates projections highlighting main structural motifs of $NH_4[Cu(HCOO)_3]$ at various temperatures: 120, 230, and 355 K.

Differential Scanning Calorimetry. Previous calorimetric study of $NH_4[Cu(HCOO)_3]$ indicated the presence of the reversible phase transition at 353 K of the first-order type, which occurs between the low-temperature orthorhombic phase (II) and high-temperature hexagonal phase (I); as seen in Figure 2,

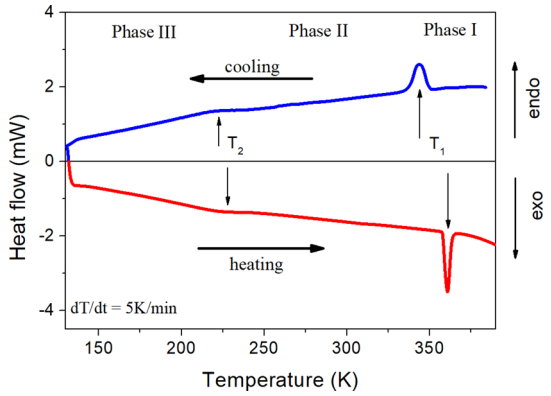

Figure 2. DSC data for $NH_4[Cu(HCOO)_3]$ between 130 and 390 K for cooling and heating run. A continuous phase transition can be seen at 225 K, and a first order phase transition can be seen at 360 K.

our DSC thermogram is in close agreement with that of a previous study (T_1 = 352 K).[16] Note that compared to the other members of an ammonium-based metal-formate family of compounds[15−19,22] this high phase transition temperature stands out, since T_c values of the corresponding phases for analogous compounds vary from 191 K (Zn analogue) to 255 K (Mg analogue). Quite intriguingly, a closer inspection of the low-temperature range in our DSC trace allows one to determine an additional heat capacity anomaly, the presence of which was not reported previously. This anomaly occurs at T_2

https://dx.doi.org/10.1021/acs.jpcc.0c06141
J. Phys. Chem. C 2020, 124, 18714−18723

= 222 K upon cooling and at 225 K upon heating, with the shape of envelope suggesting a continuous character of the transition. It is worth noting that the observed excess specific heat anomaly at 225 K is small and smeared, which makes difficult the identification of its order. However, the small thermal hysteresis suggests that the phase transition is of the second-order type (see Figure 3a). In the high temperature region, the observed

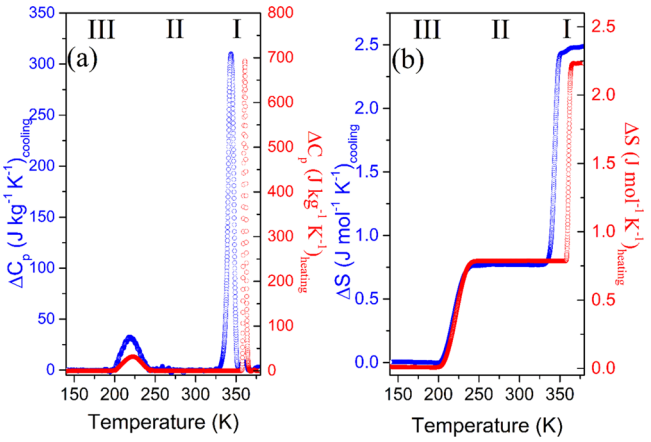

Figure 3. Changes in (a) heat capacity and (b) entropy related to the phase transitions in $NH_4[Cu(HCOO)_3]$.

excess specific heat at 352 K has a symmetric shape, indicating the first-order phase transition, which is consistent with previously reported results.

The associated changes in entropy values ΔS are estimated to be about 1 and 1.5 J mol^{-1} K^{-1} for T_2 and T_1, respectively (Figure 3b). For an order−disorder transition, $\Delta S = R\ln(N)$, where R is the gas constant and N is the ratio of the number of configurations in the disordered and ordered phase. Taking the ΔS estimated from DSC analysis, the value of the N parameter for T_2 is estimated to be equal to 1; hence, the symmetry is retained upon the II → III phase transition (an isostructural phase transition). For high-temperature phase transition T_1, the estimated value of N is approximately equal to 1.5, confirming the order−disorder character of the phase transition. These results are in agreement with structural data obtained from X-ray diffraction, where it was shown that the NH_4^+ ions occupy six disordered sites in phase I ($N_I = 6$) and four unique sites in phase II ($N_{II} = 4$).[18]

Raman Spectroscopy. Raman spectra plotted as a function of temperature for $NH_4[Cu(HCOO)_3]$ are presented in Figure 4 and Figure S2 in the Supporting Information. Understanding of the collected spectra may be facilitated by dividing the Brillouin zone-center vibrations into internal vibrations of the ammonium ions and formate ions and the lattice vibrations. The free formate ion, hereafter referred to (F), has C_{2v} symmetry with six fundamental vibrations divided into the CH stretching (ν_{1F}), the symmetric CO stretching (ν_{2F}), the antisymmetric CO stretching (ν_{4F}), the symmetric OCO bending (ν_{3F}), the in-plane CH bending (ν_{5F}), and the out of plane CH bending (ν_{6F}) mode.[23,24] The free ammonium (A) cation has T_d symmetry and exhibits only four internal vibrations: the symmetric stretching (ν_{1A}), the symmetric bending (ν_{2A}), the antisymmetric stretching (ν_{3A}), and the antisymmetric bending (ν_{4A}) mode.[25] The proposed assignment of the observed internal and external (T' and L denote translational and librational modes, respectively) Raman bands (Table 1) is based on the rich literature data for formate-based MOFs, as well as on the DFT calculations performed for $[NH_4]Na_{0.5}Cr_{0.5}(HCOO)_3$, therefore, they are not discussed in this paper.[14,23,24]

$NH_4[Cu(HCOO)_3]$ adopts the $P2_12_12_1$ orthorhombic symmetry (phase II) at room temperature with four formulas per primitive cell. Thus, according to the factor group analysis, the total number of expected modes corresponding to formate ions increases to 144 (36A + 36B_1 + 36B_2 + 36B_3), ammonium ions to 60 (15A + 15B_1 + 15B_2 + 15B_3), and Cu^{2+} ions to 12 (3A + 3B_1 + 3B_2 + 3B_3), as presented in Table S4 in the Supporting Information. Since all symmetry optical species (54A + 53B_1 + 53B_2 + 53B_3) are Raman-active for this symmetry, the total number of expected Raman bands is equal to 216. The increase of temperature above 355 K leads to the symmetry trans-

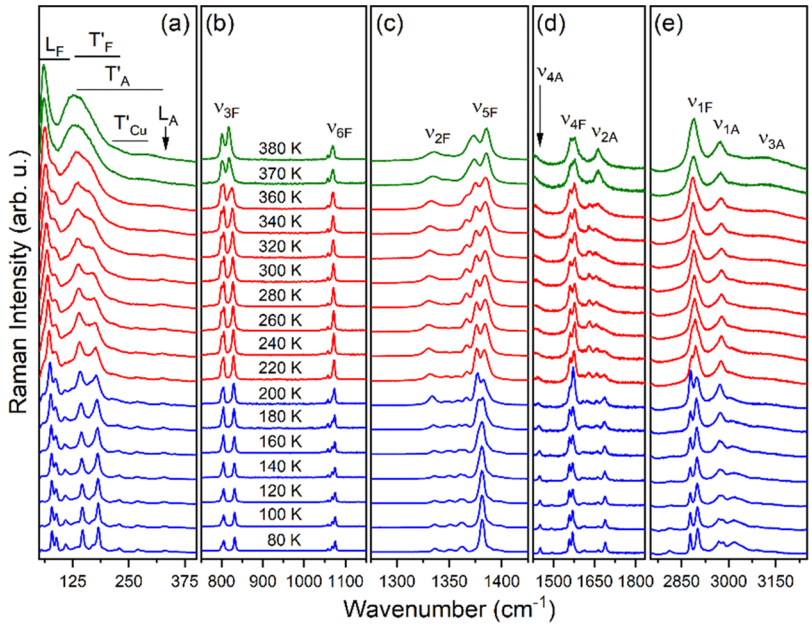

Figure 4. Temperature-dependent Raman spectra of $NH_4[Cu(HCOO)_3]$.

https://dx.doi.org/10.1021/acs.jpcc.0c06141
J. Phys. Chem. C 2020, 124, 18714−18723

Table 1. Assignments of Observed Raman Bands for $NH_4[Cu(HCOO)_3]$ at 80, 300 (RT), and 380 K[a]

phase III (80 K)	phase II (RT)	phase I (380 K)	assignment
3258_w, 3198_{sh}, 3140_{sh}, 3087_w, 3047_{sh}, 3016_w	3107_w, 3018_{sh}	3116_m, 3020_{sh}	ν_{3A}
2984_w, 2969_w	2976_m	2971_m	ν_{1A}
2901_m, 2878_m	2889_s	2888_{vs}	ν_{1F}
2811_w, 2789_{sh}, 2757_{vw}, 2722_{vw}	2755_w, 2717_{vw}	2754_w, 2720_{vw}	$\nu_{3A} + \nu_{1A}$
1689_w, 1663_{vw}, 1619_{vw}	1678_{sh}, 1656_w, 1630_{vw}	1664_w	ν_{2A}
1570_w, 1557_w	1577_w, 1559_w	1576_w, 1561_w	ν_{4F}
1452_{vw}			ν_{4A}
1400_{vw}, 1395_{vw}, 1389_{sh}, 1381_{vs}, 1363_m, 1361_m	1384_{vs}, 1375_s, 1366_m	1386_{vs}, 1373_s	ν_{5F}
1351_w, 1336_w	1331_w	1336_m	ν_{2F}
1076_w, 1068_{vw}, 1058_{vw}	1071_w, 1057_{vw}	1069_w, 1058_{vw}	ν_{6F}
832_w, 805_w, 795_{sh}	827_w, 806_w, 799_w	818_w, 801_w	ν_{3F}
331_{vw}	327_{vw}		L_A
283_{vw}, 270_w, 229_w, 217_{sh}	280_{vw}, 222_{sh}	295_w	$T'_A + T'_{Cu}$
195_{sh}, 182_w, 172_{sh}, 145_w, 132_{vw}	167_m, 135_m	142_{sh}	$T'_A + T'_F$
110_w, 89_w, 79_w	105_{sh}, 84_m, 66_m	116_m, 62_s	L_F

[a]Key: vs, very strong; s, strong; m, medium; w, weak; vw, very weak; sh, shoulder.

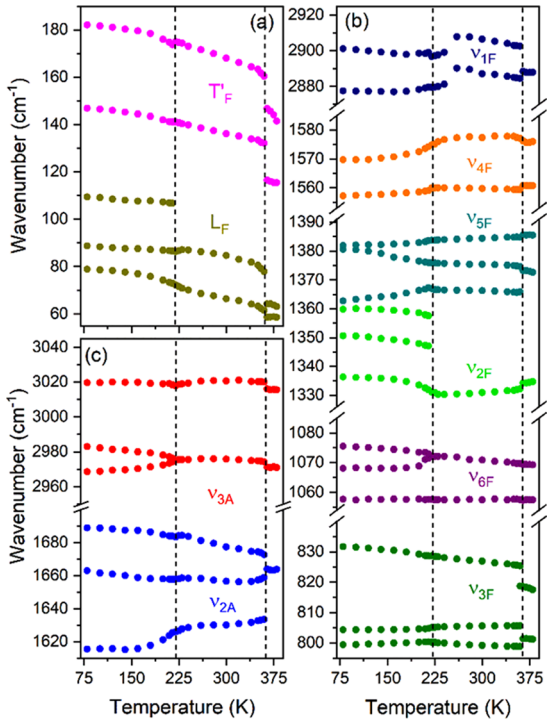

Figure 5. Positions of selected Raman bands as a function of temperature.

formation to the $P6_122$ hexagonal symmetry (phase I) with a larger primitive cell accommodating six formulas and disordered NH_4^+ cations.[16] Such an extension of the unit cell leads to the further increase of expected vibrational modes corresponding to formate ions to 216 ($17A_1 + 19A_2 + 17B_1 + 19B_2 + 36E_1 + 36E_2$), ammonium ions to 90 (irreducible representation remains unknown due to their disorder), and Cu^{2+} ions to 18 ($A_1 + 2A_2 + 2B_1 + B_2 + 3E_1 + 3E_2$). Although the total number of optical modes for phase I is as high as 321, only the A_1, E_1, and E_2 species are Raman-active; therefore, the total number of expected Raman bands is significantly lower in comparison to phase II, i.e., 89 ($17A_1 + 36E_1 + 36E_2$) for formate ions and 6 ($A_1 + 2E_1 + 3E_2$) for modes involving Cu^{2+} ions.

Our Raman data (Figure 4, Figure S2 in the Supporting Information and Table 1) clearly show merging or vanishing of bands upon heating up to 365 K, confirming the increase of symmetry upon transition to hexagonal phase I. These changes are well-reflected in Figure 5 presenting the positions of bands as a function of temperature. Sudden jumps at 365 K confirm that the observed phase transition has a first-order nature, while significant broadening of bands upon heating confirms that phase I is highly disordered. The strongest changes of the full width at half maximum (FWHM) parameter are observed for bands corresponding to NH_4^+ cations, which is in good agreement with previously reported XRD data showing their dynamic disorder in phase I.[16]

It is well-known that Raman spectroscopy can detect very subtle and local structural changes that can remain unnoticed by XRD techniques. Indeed, the previously reported crystal data presented for $NH_4[Cu(HCOO)_3]$ did not clearly point to any other structural phase transition down to 94 K.[16] Our Raman spectra, however, show distinct anomalies at 220 K upon cooling that are attributable to the transformation of the continuous type (labeled as phase III). This hypothesis is supported by the emergence and/or splitting of bands as well as in changes of their relative intensities upon cooling.

Assuming that the crystal symmetry is retained in phases II and III, we focus on the oxygen environment of the central metal ions and HB network, since the observed Raman anomalies are strongly manifested for bands corresponding to these structural components. This behavior suggests that both the NH_4^+ ions and metal-formate framework participate in this phase transition and the copper-formate framework is more distorted in phase III. For the needs of the present paper, we recollected XRD data with a finer temperature step and compared with those obtained by Shang et al.[16] The results are presented in Figure 6; atom

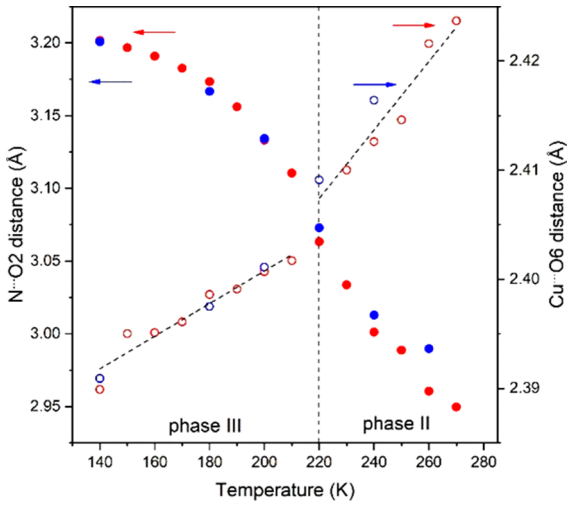

Figure 6. Change in the N···O2 (full symbols) and Cu···O6 (open symbols) distances plotted as a function of temperature based on our experiments (red color) and compared to literature data (blue color),[12] and the dashed lines represent linear fit to our data.

https://dx.doi.org/10.1021/acs.jpcc.0c06141
J. Phys. Chem. C 2020, 124, 18714−18723

labeling is supplied in Figure S3 in the Supporting Information. According to both datasets, a steplike change in the longest Cu−O6 distance near 220 K is present (Figure 6). This observation points to the fact that a change in the magnitude of the Jahn-Teller effect experienced by the CuO_6 subnetwork occurs. In turn, this influences the geometry and strength of the created HBs and forces the rearrangement of NH_4^+ cations to optimize their positions within the modified crystal voids; for example, the N1—HD···O6^{iii} HB noticeably changes its geometrical parameters, and the N1−O6 distance shortens from 2.906(3) at 230 K to 2.870(2) at 120 K (for the whole dataset, see tabulated values in Table S3 in the Supporting Information).

We also found that the subsequent extension of the unit cell along the *a* and *b* axes (followed by shrinking along the *c* axis) upon heating leads to the decreased separation of the N···O2 distance (Figure 5) at about 230 K. The clear inflection of this function at 220 K suggests that both effects take place simultaneously.

The elongation (distortion) of CuO_6 octahedra, the distortion of the copper-formate framework, and arrangement of HBs are cooperative effects and contribute to significant changes in Raman bands involving formate ions near 220 K (Figure S4 in the Supporting Information) as well as to strong narrowing of bands originating from NH_4^+ cations. The very pronounced changes in the lattice mode region serve as additional proofs of the occurring phase transition at 220 K. The emergence of new bands or their splitting below 220 K is rather attributed to symmetry changes of building blocks and narrowing of bands, allowing for their better separation upon cooling.

Dielectric Properties. The observed structural transitions in the low-temperature range are relatively subtle due to their Jahn-Teller character but are expected to have an impact on the dielectric properties in both temperature and frequency domains. Also, the first-order phase transition in the high-temperature range should be reflected in the dielectric data. Thus, to probe the relaxation dynamics of $\mathbf{NH_4[Cu(HCOO)_3]}$, we performed broadband dielectric spectroscopy measurements on a single-crystal sample oriented along the [011] direction in the 10^{-1}−10^6 Hz frequency range and in a broad temperature range of 130−390 K covering phases I−III.

The temperature dependence of both the real and imaginary parts of the complex dielectric permittivity is presented in Figure 7 for various frequencies. Dielectric results show clear changes in the slope in the vicinity of the low-temperature phase transition temperature at which DSC anomaly was observed. In a low-temperature range (the zoomed-in range of 170−250 K is provided as an inset), the ε' increases monotonically with the increasing temperature, taking relatively small values of ca. 38 (depending on frequency) at a phase transition temperature of about 225 K. Upon further heating, above 225 K, ε' values exhibit a plateau region (or even small lowering for higher frequencies) up to temperatures equal ca. 260 K. On the other hand, it should be noted that at high temperatures, a trace of the next phase transition at 352 K cannot be noticed.

For higher temperatures, ε' systematically increases. The shape of $\varepsilon'(T)$ dependence indicates the existence of the dipolar relaxation process that moves to higher temperatures with frequency. This conclusion is corroborated by the emergence of the relaxation process in the $\varepsilon''(T)$ plot, visible as a peak, in the same temperature range (Figure 7b). Only marked bending up at the highest temperature points indicates a contribution from the electrode polarization effect (Figure 7a). Similarly, an upward trend in the $\varepsilon''(T)$ plot in the high temperature range is

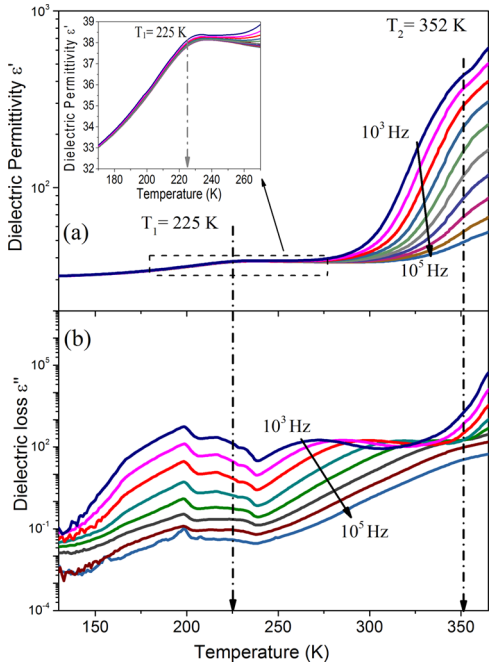

Figure 7. (a) Dielectric permittivity and (b) dielectric loss plotted as a function of temperature in $\mathbf{NH_4[Cu(HCOO)_3]}$. Dashed lines correspond to the structural phase transition temperatures. The low temperature region was enlarged and is presented in the inset.

attributed to the dc-conductivity mixed with the electrode polarization, e.g., for ε'' spectra collected for 10^3 Hz, this increase is visible only for temperatures starting from ca. 310 K and shifts to higher temperatures with frequency, see Figure 7b. However, the dipolar relaxation process reflected in the temperature dependence of both the ε' and ε'' is rather broad; hence, it was difficult to reliably estimate its characteristic relaxation times.

To resolve this issue, the ε' and ε'' were transformed to the frequency domain. In this representation, the dipole relaxation process was better visible for the temperature one (Figure 8a,b). To parameterize the relaxation process, the Cole−Cole (CC) equation with a conductivity term was employed,

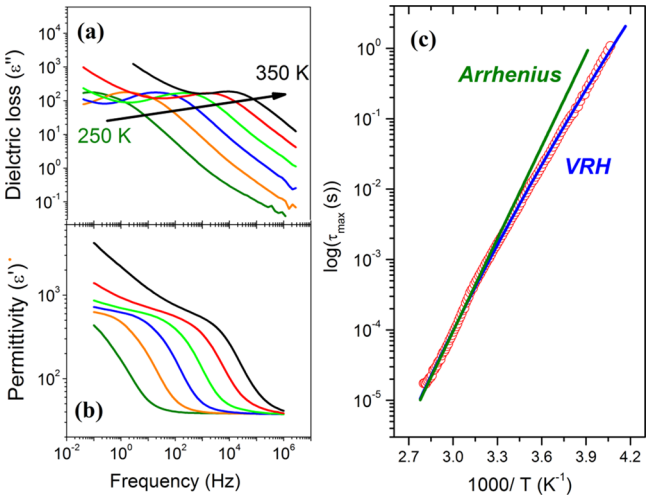

Figure 8. (a) Relaxation map, τ as a function of $1000/T$. Frequency dependence of (b) imaginary and (c) real component spectra of complex dielectric permittivity. Blue line represents the VRH fit of the whole data set. Green line is the guide for the eyes.

https://dx.doi.org/10.1021/acs.jpcc.0c06141
J. Phys. Chem. C 2020, 124, 18714−18723

$\varepsilon''(\omega) = \mathrm{Im}\left(\varepsilon_\infty + \frac{\Delta\varepsilon_i}{1+(i\omega\tau)^\alpha}\right) + \frac{\sigma_{DC}}{\varepsilon_0\omega^{-s}}$, where ε_∞ is the high-frequency dielectric constant, $\Delta\varepsilon_i$ is the dielectric strength, τ is the dielectric relaxation time, α is the shape parameter describing symmetrical broadening of the relaxation curve in comparison to the exponential-in-shape Debye relaxation, σ_{DC} is the dc-conductivity, and s is the slope parameter (see Figure S5). The inverse temperature dependence of the determined mean relaxation time of the dipolar relaxation is shown in Figure 8c. At first sight, it may appear that the $\log\tau(T^{-1})$ plot reveals a linear temperature behavior. In this scenario, relaxation corresponds to a thermally activated Arrhenius process for which $\tau = \tau_0 \exp(E_a/kT)$ (where E_a and τ_0 denote the activation energy and attempt time, respectively, and k is the Boltzmann constant). The linear fit to the experimental data provided E_a = 0.76(2) eV. The obtained value of the activation energy is much larger than the value of 0.28 eV reported for $[NH_4][Mg(HCOO)_3]$[15] and 0.17 eV reported for $[NH_4][Zn(HCOO)_3]$.[14] This result may indicate that the ammonium cation is strongly bonded to the copper formate framework compared to the magnesium and zinc-based analogues and breaking of its position requires much more energy. Nevertheless, a closer inspection of the $\log\tau(T^{-1})$ plot reveals that there is an essentially nonlinear T^{-1}-dependence with a convex curvature, indicating temperature-dependent activation energy of τ (deviation of the green solid line from the experimental data points in Figure 8c).

One way to parametrize a characteristic curvature of $\tau(T^{-1})$ dependency is to employ the VRH model[26,27] $\tau(T) = \tau_0 \exp\left(\frac{T_0}{T}\right)^{1/4}$. Least-squares fitting of experimental data to this equation afforded a T_0 value equal to 6.1×10^{10} K. It is related to the disorder energy, which in our case corresponds to variations in the local environment of the small NH_4^+cation participating in the hopping process inside crystal lattice cavities.[28]

SHG Properties and Unusual Switching between Two SHG-Active States. A reliable way to establish if a given crystalline material features noncentrosymmetric setting is to probe whether it exhibits second-order nonlinear optical phenomena upon irradiation with high-intensity laser pulses. Among these phenomena, the most widely examined one for that purpose is the frequency mixing in its degenerate variant—the second harmonic generation (SHG). Given the relatively high sensitivity of SHG to structural changes, it can be used to monitor temperature-induced phase transitions.[29−33] Accordingly, we have used the temperature-resolved second harmonic generation (TR-SHG) technique in order to gather broader evidence on the lattice, a centricity of I and II crystal phases of $\mathbf{NH_4[Cu(HCOO)_3]}$. To that end, we have irradiated the sieved sample of $\mathbf{NH_4[Cu(HCOO)_3]}$ (particle size distribution of 88−125 μm) with 1250 nm, 130 fs laser pulses of 99 mW mean power from 298 to 373 K (heating run) and from 373 to 298 K (cooling run) with a 2−3 K step. Figure 8 presents integral intensities of SHG signals for heating and cooling runs plotted vs temperature, while corresponding spectra of the second harmonic of radiation are provided in the Supporting Information (Figures S6 and S7 in the Supporting Information).

Upon heating, the SHG response gradually decreases down to 353 K at which point it experiences an approximately six-fold decrease in intensity due to phase transition II → I. Clearly, the second harmonic response is present above the phase transition temperature (see Figures S6 and S7 in the Supporting Information), and hence, this transition has a confirmed noncentrosymmetric character. Further heating of the sample up to 378 K does not lead to significant changes in the integral intensity of SHG. During cooling run, no apparent changes occur down to 354 K. Beyond that point, SHG signal rises in intensity ca. five times, which attests to the reversibility of investigated phase transition.

Moreover, to get a more quantitative grasp on the efficiency of SHG, we have also conducted the Kurtz-Perry powder test[20,21] at two wavelengths: 1250 nm and 800 nm. This test was conducted at 298 K; thus, relative conversion efficiencies (expressed as the fraction of integral intensities of the obtained SHG signal of $\mathbf{NH_4[Cu(HCOO)_3]}$ and that of the reference KDP sample, both of the same particle size distribution) describe the properties of the room temperature phase II. We found that relative SHG efficiency is equal to 0.081 vs KDP when using 1250 nm pumping wavelength and 0.058 vs KDP when 800 nm is used (Figures S8 and S9 in the Supporting Information). Note that relative SHG efficiencies of that order can be considered quite high if one appreciates that this material has a high content of Cu^{2+} centers; hence, its absorption bands are likely to attenuate the resulting second harmonic response. Indeed, comparatively lower SHG activity at 800 nm is ascribable to the self-absorption phenomenon, referred also to as the 'filtering effect'.[34] In the case of $\mathbf{NH_4[Cu(HCOO)_3]}$, one can note that an 800 nm laser line falls within the Cu^{2+} absorption band that resides in the red portion of the electromagnetic spectrum, decreasing, in this manner, the intensity of the resulting second harmonic of radiation. We have also observed that prolonged exposure of $\mathbf{NH_4[Cu(HCOO)_3]}$ to 800 nm irradiation leads to its photochemical decomposition, the origin of which we see indirect, intense pumping of the Cu^{2+} absorption band.

The TR-SHG results presented above leave no doubt that crystal phases I and II of $\mathbf{NH_4[Cu(HCOO)_3]}$ are both acentric. A first-order character of the phase transition between phases I and II and ca. 6-fold difference in SHG intensity opens up the question whether this material can be employed as a bistable NLO switch operating between two SHG-active states: SHG-*high* (phase II) and SHG-*low* (phase I). In order to investigate whether this is a viable possibility, the cycling experiment was performed, i.e., $\mathbf{NH_4[Cu(HCOO)_3]}$ was irradiated with 1250 nm femtosecond laser pulses, and the temperature was alternated between two temperature points, 346 and 364 K. Note that TR-SHG traces (Figure 9) indicate a hysteretic behavior of the SHG response. Accordingly, in order to be sure that the temperature-induced conversion between distinct phases will take place after each heating/cooling cycle, quite large separation of 18 K was chosen to realize the SHG switching experiment.

A plot of integral intensities of SHG collected during the switching experiment is presented in Figure 10a, and the corresponding experimental spectra of the SHG signal are displayed in Figure 10b. It is apparent that while there is some downward drift of the observed SHG intensity over seven consecutive heating and cooling runs, the second harmonic intensity is generally stable; also, the contrast ratio of the SHG signal of SHG-*high* (phase II) and SHG-*low* (phase I) remains ca. 6-fold, which is in accordance with TR-SHG data (Figure 8). This result demonstrates that the transition between phases I and II of $\mathbf{NH_4[Cu(HCOO)_3]}$ is reversible, but most importantly, this indicates that this material is a promising

https://dx.doi.org/10.1021/acs.jpcc.0c06141
J. Phys. Chem. C 2020, 124, 18714−18723

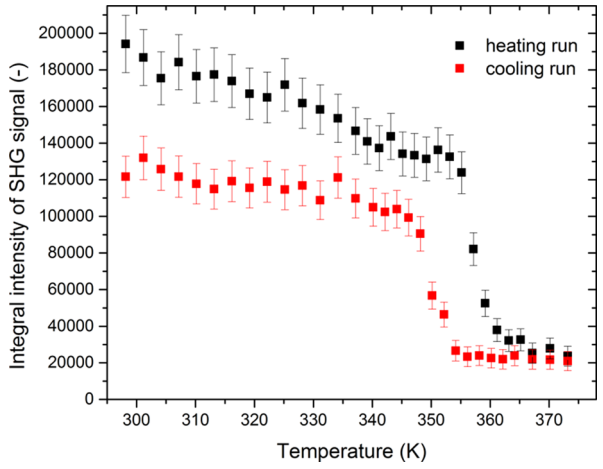

Figure 9. Integral intensities of SHG signals of $\mathbf{NH_4[Cu(HCOO)_3]}$ for heating (298−373 K) and cooling (373−298 K) runs plotted as a function of temperature.

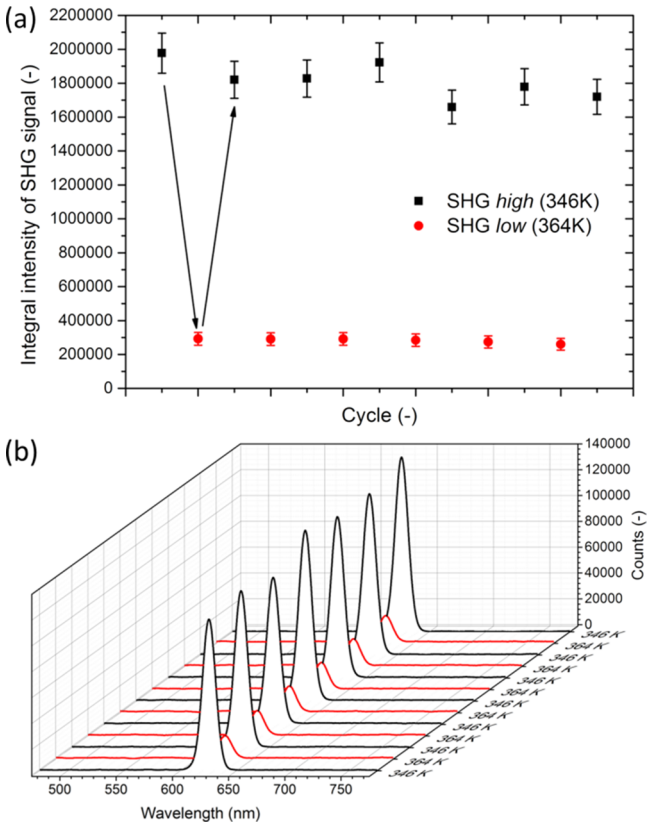

Figure 10. (a) Plot of integral intensities of SHG collected during the switching experiment at 346 K (black squares) and 364 K (red circles). (b) Experimental spectra of the SHG signal obtained during the switching experiment. Spectra were collected at 346 K (black traces) and 364 K (red traces).

candidate for temperature-induced switching of the SHG response.

What sets the title compound apart from the vast majority of known SHG switches is that it allows for switching of NLO responses between two distinct, yet both SHG-active states (switching of SHG-*high* − SHG-*low* type). An additional advantage is that switching between SHG-active phases takes place above room temperature. Indeed, if one looks what is the most common variant of temperature-driven SHG switching, it becomes clear that almost all known NLO switches take advantage of phase transitions between noncentrosymmetric and centrosymmetric crystal phases, thus narrowing the available set of NLO responses into two binary variants: SHG-*on* and SHG-*off*.[30,35−39] At present, there is ca. twenty examples of SHG switches of this kind, including those operating at room temperature and above.[40−44] There are also single examples of more complicated switching sequences of binary SHG outputs, e.g., SHG-*off* − SHG-*on* − SHG-*off* in the case of $[C_4H_{10}N][CdCl_3]$, with T_{c1} and T_{c2} of 218 and 241 K, respectively.[45]

$\mathbf{NH_4[Cu(HCOO)_3]}$ should be compared to extant examples of NLO switches, which also employ two SHG-active states. In fact, there are only three materials for which switching behavior of this kind was unequivocally proven. A very recent example is lead-halide perovskite material of the formula $MHyPbCl_3$ (MHy stands for methylhydrazinium cations), which features SHG switching of the SHG-*low* − SHG-*high* type[46] (T_c at 342 K), i.e., high-temperature phase revealed enhanced SHG activity compared to the low-temperature phase; hence, its SHG states are in reverse order than in $\mathbf{NH_4[Cu(HCOO)_3]}$. Acid−base adducts $NH_4[(CH_3)_4N]SO_4{\cdot}H_2O$[47]and $[(C_3H_7)_2NH_2][CCl_3COO]$[48] were found to reveal two-step SHG switching in which first two phases (low-temperature) are SHG-active, whereas the high-temperature phase is SHG-inactive (SHG-*high* − SHG-*low* − SHG-*off* sequence). Accordingly, by contrast to $\mathbf{NH_4[Cu(HCOO)_3]}$, which is a bistable NLO switch, these materials belong to the family of tristable switches, as they offer an additional transition to the centrosymmetric phase. A common feature of these switches is that they operate at relatively low temperatures (T_{c1} = 169 K, T_{c2} = 204 K and T_{c1} = 142 K and T_{c2} = 228 K, respectively).

CONCLUSIONS

In this work, a comprehensive set of experimental techniques was used to probe the order−disorder phase transition in a perovskite-like copper-formate framework $\mathbf{NH_4[Cu(HCOO)_3]}$. This study served as a window to an understanding of the mechanism of the phase transition. In particular, we have examined the role of the Jahn−Teller effect of Cu^{2+} ions. Temperature-dependent studies confirmed the presence of phase transition at T_2 = 353 K and the additional phase transition at T_1 = 222 K, which was not characterized in detail previously. Our data confirm the postulated continuous nature of low-temperature phase transition, whereas Raman data and thermal studies lead us to the conclusion that the transition at 355 K between orthorhombic (II) and hexagonal (I) phases is of the first-order type. Low-temperature Raman data were analyzed in the context diffraction results, and the observed changes of Raman shifts can be explained by taking into account the significant effect of Jahn−Teller distortion on the vibrational properties of the CuO_6 subnetwork. The dynamics of $\mathbf{NH_4[Cu(HCOO)_3]}$ were also investigated using broadband dielectric spectroscopy for single crystals. Dielectric investigations revealed the symmetric shape of the Cole−Cole relaxation function describing the relaxation process. The obtained E_a value of approximately 0.76 eV is related to the variation in the local environment of small NH_4^+cations inside cavities of the crystal lattice sites. Finally, TR-SHG studies confirmed acentric setting of phases II and I, as well as allowed us to realize an uncommon kind of temperature-induced switching of the second-order NLO response between two SHG-active states: SHG-*high* state below T_c, and SHG-*low* state above T_c. This kind

https://dx.doi.org/10.1021/acs.jpcc.0c06141
J. Phys. Chem. C 2020, 124, 18714−18723

of SHG bistability is unusual in the context of extant molecular and coordination polymer NLO switches, which operate almost exclusively between binary states: SHG-*on* and SHG-*off*.

■ ASSOCIATED CONTENT

Supporting Information

The Supporting Information is available free of charge at https://pubs.acs.org/doi/10.1021/acs.jpcc.0c06141.

Complementary data including crystallographic tables, selected interatomic distances and angles, selected hydrogen-bond parameters, thermal evolution of lattice parameters, additional projection of the crystal structure, Raman spectra and Raman shift assignments, frequency dependence of the dielectric loss, TR-SHG data, and room temperature spectra of SHG (PDF)

Crystallographic data for $\mathbf{NH_4[Cu(HCOO)_3]}$ collected at 120 K (CIF)

Crystallographic data for $\mathbf{NH_4[Cu(HCOO)_3]}$ collected at 230 K (CIF)

■ AUTHOR INFORMATION

Corresponding Authors

Jan K. Zaręba − *Advanced Materials Engineering and Modelling Group, Wrocław University of Science and Technology, 50-370 Wrocław, Poland;* orcid.org/0000-0001-6117-6876; Email: jan.zareba@pwr.edu.pl

Adam Sieradzki − *Department of Experimental Physics, Wrocław University of Science and Technology, 50-370 Wrocław, Poland;* orcid.org/0000-0003-4136-5754; Email: adam.sieradzki@pwr.edu.pl

Authors

Paulina Peksa − *Department of Experimental Physics, Wrocław University of Science and Technology, 50-370 Wrocław, Poland*

Maciej Ptak − *Institute of Low Temperature and Structure Research, Polish Academy of Sciences, 50-950 Wrocław, Poland;* orcid.org/0000-0002-4639-2367

Mirosław Mączka − *Institute of Low Temperature and Structure Research, Polish Academy of Sciences, 50-950 Wrocław, Poland;* orcid.org/0000-0003-2978-1093

Anna Gągor − *Institute of Low Temperature and Structure Research, Polish Academy of Sciences, 50-950 Wrocław, Poland*

Sebastian Pawlus − *Institute of Physics, University of Silesia, 41-500 Chorzów, Poland;* orcid.org/0000-0001-9209-4056

Complete contact information is available at: https://pubs.acs.org/10.1021/acs.jpcc.0c06141

Author Contributions

The manuscript was written through contributions of all authors. All authors have given approval to the final version of the manuscript.

Notes

The authors declare no competing financial interest.

■ ACKNOWLEDGMENTS

The authors are deeply grateful for financial support by the National Science Centre within the framework of the Opus13 project (Grant No. DEC-2017/25/B/ST3/02321).

■ REFERENCES

(1) Mączka, M.; Almeida da Silva, T.; Paraguassu, W.; Pereira da Silva, K. Raman Scattering Studies of Pressure-induced Phase Transitions in Perovskite Formates $[(CH_3)_2NH_2][Mg(HCOO)_3]$ and $[(CH_3)_2NH_2][Cd(HCOO)_3]$. *Spectrochim. Acta A* **2016**, *156*, 112−117.

(2) Zhou, H.-C.; Long, J. R.; Yaghi, O. M. Introduction to Metal−Organic Frameworks. *Chem. Rev.* **2012**, *112*, 673−674.

(3) Janiak, C.; Vieth, J. K. MOFs, MILs and More: Concepts, Properties and Applications for Porous Coordination Networks (PCNs). *New J. Chem.* **2010**, *34*, 2366−2388.

(4) Wang, Z.; Hu, K.; Gao, S.; Kobayashi, H. Formate-Based Magnetic Metal-Organic Frameworks Template by Protonated amines. *Adv. Mater.* **2010**, *22*, 1526−1533.

(5) Smoleński, P.; Kłak, J.; Nesterov, D. S.; Kirillov, A. M. Unique Mixed-Valence Cu(I)/Cu(II) Coordination Polymer with New Topology of Bitubular 1D Chains Driven by 1,3,5-Triaza-7-phosphaadamantane (PTA). *Cryst. Growth Des.* **2012**, *12*, 5852−5857.

(6) Karabach, Y. Y.; Kirillov, A. M.; Haukka, M.; Sanchiz, J.; Kopylovich, M. N.; Pombeiro, A. J. L. Multicopper(II) Pyromellitate Compounds: Self-Assembly Synthesis, Structural Topologies, and Magnetic Features. *Cryst. Growth Des.* **2008**, *8*, 4100−4108.

(7) Rogez, G.; Viart, N.; Drillon, M. Multiferroic Materials: The Attractive Approach of Metal−Organic Frameworks (MOFs). *Angew. Chem., Int. Ed.* **2010**, *49*, 1921−1923.

(8) Mączka, M.; Pietraszko, A.; Macalik, L.; Sieradzki, A.; Trzmiel, J.; Pikul, A. Synthesis and Order−Disorder Transition in a Novel Metal Formate Framework of $[(CH_3)_2NH_2]Na_{0.5}Fe_{0.5}(HCOO)_3$. *Dalton Trans.* **2014**, *43*, 17075−17084.

(9) Besara, T.; Jain, P.; Dalal, N. S.; Kuhns, P. L.; Reyes, A. P.; Kroto, H. W.; Cheetham, A. K. Mechanism of the Order-Disorder Phase Transition, and Glassy Behavior in the Metal-organic Framework $[(CH_3)_2NH_2]Zn(HCOO)_3$. *Proc. Nat. Acad. Sci.* **2011**, *108*, 6828−6832.

(10) Mączka, M.; Szymborska-Małek, K.; Ciupa, A.; Hanuza, J. Comparative Studies of Vibrational Properties and Phase Transitions in Metal-Organic Frameworks of $[NH_4][M(HCOO)_3]$ with M=Mg, Zn, Ni, Fe, Mn. *Vib. Spectr.* **2015**, *77*, 17−24.

(11) Fu, D.-W.; Zhang, W.; Cai, H.-L.; Zhang, Y.; Ge, J.-Z.; Xiong, R.-G.; Huang, S. D.; Nakamura, T. A multiferroic perdeutero metal-organic Framework $[(CD_3)_2ND_2][Co(DCOO)_3]$. *Angew. Chem., Int. Ed.* **2011**, *50*, 11947−11951.

(12) Sieradzki, A.; Mączka, M.; Simenas, M.; Zaręba, J. K.; Gągor, A.; Balciunas, S.; Kinka, M.; Ciupa, A.; Nyk, M.; Samulionis, V.; Banys, J.; Paluch, M.; Pawlus, S. On the Origin of Ferroelectric Structural Phases in Perovskite-like Metal−Organic Formate. *J. Mater. Chem. C* **2018**, *6*, 9420−9429.

(13) Guo, M.; Cai, H.-L.; Xiong, R.-G. Ferroelectric Metal Organic Framework (MOF). *Inorg. Chem. Commun.* **2010**, *13*, 1590−1598.

(14) Mączka, M.; Ptak, M.; Macalik, L. Infrared and Raman Studies of Phase Transitions in Metal-Organic Frameworks of $[(CH_3)_2NH_2][M(HCOO)_3]$ with M=Zn, Fe. *Vib. Spectr.* **2014**, *71*, 98−104.

(15) Mączka, M.; Pietraszko, A.; Macalik, B.; Hermanowicz, K. Structure, Phonon Properties, and Order−Disorder Transition in the Metal Formate Framework of $[NH_4][Mg(HCOO)_3]$. *Inorg. Chem.* **2014**, *53*, 787−794.

(16) Shang, R.; Chen, S.; Wang, Z.-M.; Gao, S. A Copper−Formate Framework Showing a Simple to Helical Antiferroelectric Transition with Prominent Dielectric Anomalies and Anisotropic Thermal Expansion, and Antiferromagnetism. *Chem. − Eur. J.* **2014**, *20*, 15872−15883.

(17) Shang, R.; Xu, G.-C.; Wang, Z.-M.; Gao, S. Phase Transitions, Prominent Dielectric Anomalies, and Negative Thermal Expansion in Three High Thermally Stable Ammonium Magnesium−Formate Frameworks. *Chem. − Eur. J.* **2014**, *20*, 1146−1158.

(18) Xu, G. C.; Ma, X. M.; Zhang, L.; Wang, Z. M.; Gao, S. Disorder-Order Ferroelectric Transition in the Metal Formate Framework of $[NH_4][Zn(HCOO)_3]$. *J. Am. Chem. Soc.* **2010**, *132*, 9588−9590.

(19) Wang, Z.; Zhang, B.; Inoue, K.; Fujiwara, H.; Otsuka, T.; Kobayashi, H.; Kurmoo, M. Occurrence of a Rare $4^9{\cdot}6^6$ Structural Topology, Chirality, and Weak Ferromagnetism in the $[NH_4]$-

$[M^{II}(HCOO)_3]$ (M = Mn, Co, Ni) Frameworks. *Inorg. Chem.* **2007**, *46*, 437−445.
(20) Kurtz, S. K.; Perry, T. T. A Powder Technique for the Evaluation of Nonlinear Optical Materials. *J. Appl. Phys.* **1968**, *39*, 3798−3813.
(21) Graja, A. Production of the Second Harmonic of Light in Ammonium Pentaborate and other Powdered Piezoelectric Crystals. *Phys. Phys. Status Solidi B* **1968**, *27*, K93−K97.
(22) Xu, G. C.; Zhang, W.; Ma, X. M.; Chen, Y. H.; Zhang, L.; Cai, H. L.; Wang, Z. M.; Xiong, R. G.; Gao, S. Coexistence of Magnetic and Electric Orderings in the Metal−Formate Frameworks of $[NH_4][M(HCOO)_3]$. *J. Am. Chem. Soc.* **2011**, *133*, 14948−14951.
(23) Ptak, M.; Stefańska, D.; Gągor, A.; Svane, K. L.; Walsh, A.; Paraguassu, W. Heterometallic Perovskite-Type Metal−Organic Framework with an Ammonium cation: Structure, Phonons, and Optical Response of $[NH_4]Na_{0.5}Cr_xAl_{0.5-x}(HCOO)_3$ (x = 0, 0.025 and 0.5). *Phys. Chem. Chem. Phys.* **2018**, *20*, 22284−22295.
(24) Mączka, M.; Gągor, A.; Macalik, B.; Pikul, A.; Ptak, M.; Hanuza, J. Order-Disorder Transition and Weak Ferromagnetism in the Perovskite Metal Formate Frameworks of $[(CH_3)_2NH_2][M(HCOO)_3]$ and $[(CH_3)_2ND_2][M(HCOO)_3]$(M= Ni, Mn). *Inorg. Chem.* **2014**, *53*, 457−467.
(25) Nakamoto, K. *Infrared and Raman Spectra of Inorganic and Coordination Compounds*, Wiley-Blackwell, 2008.
(26) Hill, R. M. Variable-Range Hopping. *Phys. Stat. Sol.* **1976**, *34*, 601−613.
(27) Mott, N. F. Conduction in Non-crystalline Materials. *Philos. Mag.* **1969**, *19*, 835.
(28) Molak, A.; Paluch, M.; Pawlus, S. Electrical Properties of $Pb(Mn_{1/3}Nb_{2/3})O_3$ Ceramics Under Hydrostatic pressure: Relaxation Dynamics and Its Relation to the Subsystem of Defects. *Phys. Rev. B* **2008**, *78*, 134207.
(29) Zhang, Q.; Solanki, A.; Parida, K.; Giovanni, D.; Li, M.; Jansen, T. L. C.; Pshenichnikov, M. S.; Sum, T. C. Tunable Ferroelectricity in Ruddlesden-Popper Halide Perovskites. *ACS Appl. Mater. Interfaces* **2019**, *11*, 13523−13532.
(30) Xu, L.; Gao, J. X.; Chen, X. G.; Hua, X. N.; Liao, W. Q. A Temperature-Triggered Triplex Bistable Switch in a Hybrid Multifunctional Material: $[(CH_2)_4N(CH_2)_4]_2[MnBr_4]$. *Dalton Trans.* **2018**, *47*, 16995−17003.
(31) Wei, Y. L.; Jing, J.; Shi, C.; Ye, H. Y.; Wang, Z. X.; Zhang, Y. Unusual High-Temperature Reversible Phase Transition Containing Dielectric and Nonlinear Optical Switches in Host-Guest Supramolecular Crown Ether Clathrates. *Chem. Commun.* **2018**, *54*, 8076−8079.
(32) Wang, S. S.; Chen, X. X.; Huang, B.; Su, Y. J.; Zhang, W. X.; Zeng, M. H.; Chen, X. M. Bromocholine Bromide is a Molecular Ferroelectric with Moderate Phase Transition Temperature. *J. Mat. Chem. C* **2018**, *6*, 2221−2224.
(33) Mączka, M.; Stefańska, D.; Zaręba, J. K.; Nyk, M.; Sieradzki, A. Temperature-dependent Luminescence and Second-harmonic Generation of Perovskite-type Manganese and Cadmium Dicyanamide Frameworks Templated by Tetrapropylammonium Cations. *J. Alloys Compd.* **2020**, *821*, 153464.
(34) Zaręba, J. K.; Białek, M. J.; Janczak, J.; Nyk, M.; Zoń, J.; Samoć, M. Beyond Single Wavelength SHG Measurements: Spectrally-Resolved SHG Studies of Tetraphosphonate Ester Coordination Polymers. *Inorg. Chem.* **2015**, *54*, 10568−10575.
(35) Liao, W.-Q.; Gao, J.-X.; Hua, X.-N.; Chen, X.-G.; Lu, Y. Unusual Two-step Sequential Reversible Phase Transitions with Coexisting Switchable Nonlinear Optical and Dielectric Behaviors in $[(CH_3)_3NCH_2Cl]_2[ZnCl_4]$. *J. Mat. Chem. C* **2017**, *5*, 11873−11878.
(36) Zheng, X.; Shi, P.-P.; Lu, Y.; Zhou, L.; Gao, J.-X.; Geng, F.-J.; Wu, D.-H.; Fu, D.-W.; Ye, Q. Dielectric and Nonlinear Optical Dual Switching in an Organic−inorganic Hybrid Relaxor $[(CH_3)_3PCH_2OH][Cd(SCN)_3]$. *Inorg. Chem. Front.* **2017**, *4*, 1445−1450.
(37) Sun, Z.; Luo, J.; Zhang, S.; Ji, C.; Zhou, L.; Li, S.; Deng, F.; Hong, M. Solid-State Reversible Quadratic Nonlinear Optical Molecular Switch with an Exceptionally Large Contrast. *Adv. Mater.* **2013**, *25*, 4159−4163.
(38) Ji, C.; Sun, Z.; Zhang, S.; Zhao, S.; Chen, T.; Tang, Y.; Luo, J. A Host−Guest Inclusion Compound For Reversible Switching of Quadratic Nonlinear Optical Properties. *Chem. Commun.* **2015**, *51*, 2298−2300.
(39) Tao, K.; Wu, Z.; Han, S.; Zhang, J.; Ji, C.; Wang, Y.; Zhang, W.; Luo, J.; Sun, Z. Switchable Behaviors of Quadratic Nonlinear Optical Properties Originating from Bi-step Phase Transitions in a Molecule-based Crystal. *J. Mat. Chem. C* **2018**, *6*, 4150−4155.
(40) Chen, X.-G.; Zhang, Y.-Z.; Sun, D.-S.; Gao, J.-X.; Hua, X.-N.; Liao, W.-Q. Above Room-temperature Dielectric and Nonlinear Optical Switching Materials Based on $[(CH_3)_3S]_2[MBr_4]$ (M = Cd, Mn and Zn). *Dalton Trans.* **2019**, *48*, 11292−11297.
(41) Wu, Z.; Liu, X.; Ji, C.; Li, L.; Wang, S.; Sun, Z.; Zhang, W.; Peng, Y.; Luo, J. Above-Room-Temperature Switching of Quadratic Nonlinear Optical Properties in a Bi−halide Organic−inorganic hybrid. *J. Mat. Chem. C* **2018**, *6*, 9532−9536.
(42) Zhang, J.; Han, S.; Liu, X.; Wu, Z.; Ji, C.; Sun, Z.; Luo, J. A Lead-free Perovskite-like Hybrid with Above-Room-Temperature Switching of Quadratic Nonlinear Optical Properties. *Chem. Commun.* **2018**, *54*, 5614−5617.
(43) Liu, X.; Ji, C.; Wu, Z.; Li, L.; Han, S.; Wang, Y.; Sun, Z.; Luo, J. $[C_5H_{12}N]SnCl_3$: A Tin Halide Organic−Inorganic Hybrid as an Above-Room-Temperature Solid-State Nonlinear Optical Switch. *Chem. − Eur. J.* **2019**, *25*, 2610−2615.
(44) Sun, Z.; Chen, T.; Liu, X.; Hong, M.; Luo, J. Plastic Transition to Switch Nonlinear Optical Properties Showing the Record High Contrast in a Single-Component Molecular Crystal. *J. Am. Chem. Soc.* **2015**, *137*, 15660−15663.
(45) Xu, W.-J.; He, C.-T.; Ji, C.-M.; Chen, S.-L.; Huang, R.-K.; Lin, R.-B.; Xue, W.; Luo, J.-H.; Zhang, W.-X.; Chen, X.-M. Molecular Dynamics of Flexible Polar Cations in a Variable Confined Space: Toward Exceptional Two-Step Nonlinear Optical Switches. *Adv. Mater.* **2016**, *28*, 5886−5890.
(46) Mączka, M.; Gagor, A.; Zaręba, J. K.; Stefanska, D.; Drozd, M.; Balciunas, S.; Simėnas, M.; Banys, J.; Sieradzki, A. Three-Dimensional Perovskite Methylhydrazinium Lead Chloride with Two Polar Phases and Unusual Second-Harmonic Generation Bistability above Room Temperature. *Chem. Mater.* **2020**, *32*, 4072−4082.
(47) Liu, S.; Sun, Z.; Ji, C.; Li, L.; Zhao, S.; Luo, J. Exceptional Bi-Step Switching of Quadratic Nonlinear Optical Properties in a One-Dimensional Channel Compound. *Chem. Commun.* **2017**, *53*, 7669−7672.
(48) Ji, C.; Wang, S.; Liu, S.; Sun, Z.; Zhang, J.; Li, L.; Luo, J. Exceptional Three-Level Switching Behaviors of Quadratic Nonlinear Optical Properties in a Tristable Molecule-Based Dielectric. *Chem. Mater.* **2017**, *29*, 3251−3256.

https://dx.doi.org/10.1021/acs.jpcc.0c06141
J. Phys. Chem. C 2020, 124, 18714−18723